water

MDPI

Article

A Preliminary Sorption Study of Uranium on MnO_2 (Pyrolusite) in the Presence of Siderophore Desferrioxamine B—The Mechanism of a Ternary System

Morgan Snyder, Lucy Hunley, Jordan Stanberry, Ilana Szlamkowicz, Brandon Jones and Vasileios Anagnostopoulos *

Department of Chemistry, University of Central Florida, 4353 Scorpius St., Orlando, FL 32816, USA; snyderlmorgan@gmail.com (M.S.); lucinda.hunley@ucf.edu (L.H.); jordan.stanberry@ucf.edu (J.S.); ilana.szlamkowicz@ucf.edu (I.S.); brandon.jones@ucf.edu (B.J.)
* Correspondence: vasileios.anagnos@ucf.edu

Abstract: Manganese oxides have influential sorptive properties to efficiently sequester metals, such as uranium. Sorption can become complicated by metal chelating siderophores, which create a ternary system that is capable of multiple feasible mechanisms. This study analyzes the sorption behavior of desferrioxamine B (DFOB) and desferrioxamine D (DFOD) onto pyrolusite, β-MnO_2, in the presence of U(VI) at pHs 6 and 8. The electrostatic adsorption performance is shown to have a 23% difference between the DFOB and DFOD surface sorption at pH 6. Inner-sphere coordination was identified through hydrolysis products of succinate and acetate. Together, these behaviors indicate a ternary complex system where both metals and ligands interact with the surface. Therefore, uranium in the environment can be attenuated by the conditions of a complex configuration involving multiple species and functional groups. This mechanism needs to be considered for any future modeling or strategies involving radionuclide remediation.

Keywords: uranium; radionuclide chemistry; pyrolusite; ternary system; DFOB; siderophore; sorption mechanism; manganese oxide; U(VI)

Citation: Snyder, M.; Hunley, L.; Stanberry, J.; Szlamkowicz, I.; Jones, B.; Anagnostopoulos, V. A Preliminary Sorption Study of Uranium on MnO_2 (Pyrolusite) in the Presence of Siderophore Desferrioxamine B—The Mechanism of a Ternary System. *Water* **2023**, *15*, 3241. https://doi.org/10.3390/w15183241

Academic Editor: Laura Bulgariu

Received: 18 August 2023
Revised: 8 September 2023
Accepted: 11 September 2023
Published: 12 September 2023

1. Introduction

Radionuclide contamination is a pressing global issue that demands innovative and efficient remediation strategies. The release of radionuclides into the environment by humans occurs during varying activities, either by accident or unknowingly, through mining, fertilizer production, direct discharge to the atmosphere, below-ground weapons testing, and improper storage [1–3]. Radiotoxicity, long half-lives, ecological dangers, and severe health hazards make actinides a priority for research [4–7]. The U.S. Department of Energy (DOE) is decidedly concerned about uranium (U), as several sites are undergoing active groundwater and soil remediation due to this element [8]. Various techniques are available for remediation efforts to immobilize or remove contamination, such as chemical precipitation, adsorption, ion exchange, and bioremediation [9]. These remediation strategies are influenced by complex aquatic chemistry, including redox transformations that alter the mobility, bioavailability, and toxicity of radionuclides [10]. Remediation applications involving manganese oxide minerals have garnered significant attention in recent years due to their ability to sequester and facilitate the immobilization of radionuclides [11–13]. A reduction in highly mobile U(VI) to less soluble U(IV) species via microorganisms can result in the precipitation of U(IV) minerals, thereby limiting their migration into the environment [14]. Effective and sustainable bioremediation protecting the environment and human health is dependent on the chemical understanding of radionuclide environmental interactions with microorganisms.

The complex interplay between microorganisms, the ligands they produce, and mineral surfaces significantly impacts metal cycling and mobility in aquatic environments [15,16]. Bacteria and fungi secrete low-molecular-weight organic compounds, called siderophores, in response to environmental conditions involving iron stress [17]. Under aerobic conditions, ferric iron (Fe^{3+}) is inaccessible to microorganisms [18]. Metal chelators exhibit a high affinity for mostly insoluble Fe^{3+} to mobilize their uptake or deal with metal toxicity [19,20]. Siderophores, in particular, are not limited to iron as they have been shown to form complexes with various other environmentally significant metals, including copper, nickel, zinc, americium, plutonium, and uranium [21,22]. Metal mobility has been altered by siderophores in the environment disproportionately to their concentration, making them an overlooked key component to the fate of contaminants in the environment [23]. Desferrioxamine B (DFOB) is naturally biosynthesized by fungi and bacteria in many ecosystems as a linear siderophore with three bidentate hydroxamic acid functional groups and a terminal amine that plays a key role during environmental sorption (Figure 1) [24–27]. When chelated, the molecule has a stable, distorted octahedral geometry [28]. The charged, protonated amine is pointed away from the metal and adsorbs directly onto the surface or indirectly to the surface through water molecules [29]. A similar, less common compound is desferrioxamine D (DFOD), which was used in this study to compare and clarify sorption mechanisms. The DFOD has an amide ending group, altering the sorptive mechanisms available via negating the charged terminal group found in DFOB (Figure 1). These two compounds, DFOD and DFOB, are collectively referred to as DFO.

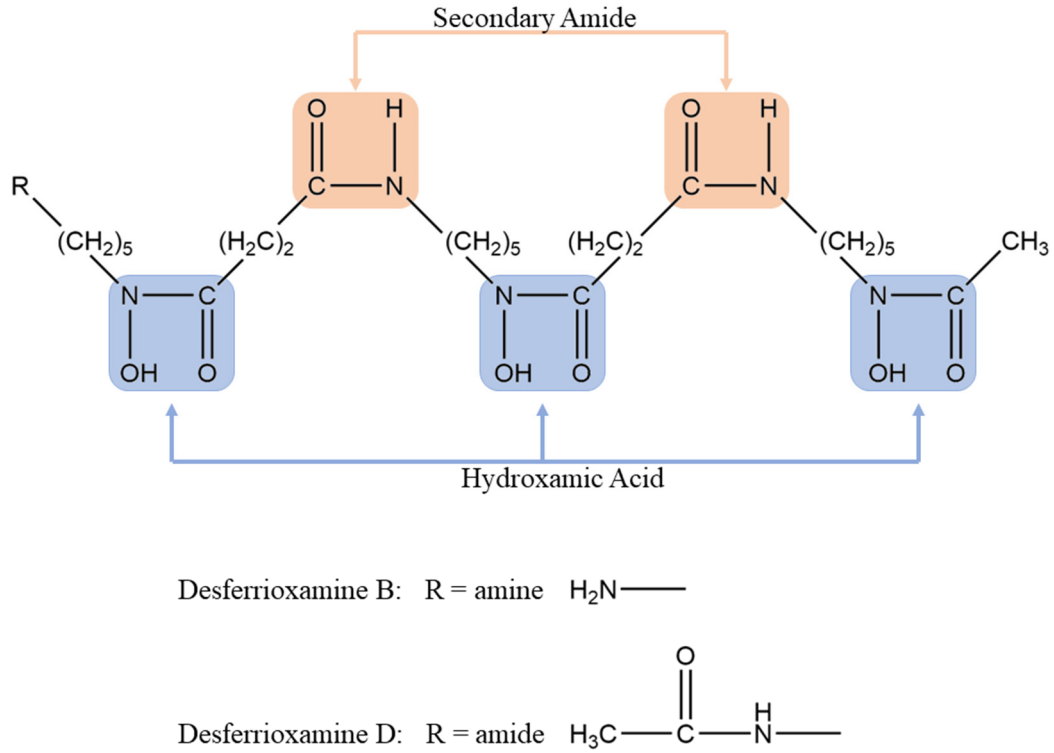

Figure 1. The structure of DFOB and DFOD shown in their neutral uncharged forms with hydroxamic acid (blue) and secondary amide (orange) groups highlighted.

Mineral surfaces can be significantly impacted by siderophores as an environmental consequence of metal production [30]. Accordingly, a comprehensive study must encompass more than binary mineral–siderophore or metal–siderophore interactions by exploring ternary metal–siderophore–mineral systems. There are over 30 oxide and hydroxide manganese types typically found in oxidation states ranging from Mn(II) to Mn(IV) [31]. Manganese oxides are ubiquitous metals in the Earth's upper crust that have a vital role in metal biogeochemical cycling [32]. As an accessible, low-cost mineral, they have been used

for robotic devices, catalysis, degradation, and energy storage [33–37]. Further, they have prominent chemical control over heavy metals at lower relative concentration proportions than more common sediments such as clay [38]. More thoroughly, there are five subclasses of MnO_2 with a structure of corner-sharing Mn(IV) octahedra interconnected with oxygen atoms and forming tunnels. Pyrolusite, β-MnO_2, is distinguished due to its noteworthy structure where each side has only one octahedron, constricting it to the smallest tunnels among the subclasses. This attribute allows for slight deviations from pure MnO_2, as the narrow tunnels are unable to accommodate other chemical species (except perhaps H^+), ensuring that the shape remains largely unaltered [39]. Pyrolusite has strong oxidative capacities to adsorb and catalyze redox reactions for a variety of metal cations [39]. The presence of DFO can further alter the adsorption and dissolution behaviors depending on the interactions between the ligand, metal, and mineral surfaces [40].

Previous articles have studied U-DFOB in the context of adsorption, mobilization, solvent extraction, and spectrophotometry [22,41–44]. However, few have continued experimentation to include the complex with minerals, and, as far as is known, none have provided a mechanism or performed environmental conditions [45–47]. This study presents an analysis of the merits of three types of mechanisms with U(VI) by comparing DFOB and DFOD at pH 6 and 8 in a manganese mineral environment. The ternary configuration utilizing multiple functional groups is supported by examining the hydrolysis of DFOB, inner-sphere coordination, and electrostatic interactions.

2. Materials and Methods

2.1. Materials

Pyrolusite, β-MnO_2, (Alfa Aesar (Ward Hill, MA, USA), 98% purity), DFOB-mesylate salt ($C_{25}H_{48}N_6O_8 \bullet CH_4O_3S$, Acros Organics (Antwerp, Belgium), 95% purity), and uranium (U(VI) ($UO_2(NO_3)_2 \bullet 6H_2O$ (Thermo Scientific (Waltham, MA, USA), 99% purity) were procured from commercial vendors. The DFOD was made via the procedure described by Kraemer et al. [48]. Dissolution created a cloudy mixture, presumably due to the slightly less soluble nature of the compound [48]. A transparent solution was created after 6 h of sonication (Digital Pro (Beijing, China), Ultrasonic Cleaner, 40 K Hz 180 W). The hydrolysis of DFOB (with a detailed explanation below) due to sorption on the substrate was identified through the amount of acetate and succinate produced, as determined by ion chromatography (Thermo Scientific, Dionex Integrion HPIC) equipped with a 4 mm anionic exchange column (Thermo Scientific, AS20), a suppressor (Thermo Scientific, Dionex ADRS 600 Suppressor), a 20 µL sample loop, and a conductivity detector (Thermo Scientific, Dionex Integrion Conductivity Detector). This instrument was operated at 1.0 mL/min with a 35 mM NaOH (Acros Organics, extra pure carbonate free) eluent and a constant voltage of 4.0 V. Mesylate ions interfered with acetate retention times (approximately 3.3 min) and was removed from DFO using an ion exchange column with Dowex 1 × 2 (Acros Organics, chloride form, 200–400 mesh), following the procedure of Simanova et al. [49]. Complete demesylation was verified by the absence of a mesylate peak at 3.4 min using ion chromatography with a 4 mm anionic exchange column using 35 mM NaOH as an eluent with a 1 mL/min flow rate. All solutions were made using ultra-pure water (Thermo Scientific, Barnstead™ GenPure™ Pro, 18.2 MΩ·cm).

2.2. U-DFO Solution Preparation

The U-DFOB complex stock solution was prepared by mixing 1 mM DFOB (demesylated) and 1 mM of U(VI) at pH 6. The U-DFOD complex was prepared with the same 1:1 ratio. The existence of the U-DFO complex was identified by the two characteristic peaks of the complex at 490 and 380 nm using a double-beam UV-Vis spectrophotometer (Thermo Scientific, Genesys 50) [41].

2.3. Sorption Experiments

Suspensions of pyrolusite were allowed to equilibrate in ultra-pure water before adsorption experiments by bringing into contact 10 mg of pyrolusite with 10 mL of ultra-pure water in 15 mL centrifuge tubes over 24 h in a tube revolver. The pH was measured (Thermo Scientific, Fisherbrand™ FE150 pH Benchtop Meter) and adjusted sporadically by adding drops of 0.1 M or 0.01 M NaOH or HCl as needed until the pH was stabilized and showed no change after 24 h. The pH values were adjusted to 6 and 8 for the experiments investigating the effect of pH. Samples were spiked with the appropriate amounts of U-DFO stock solution. For the experiments investigating the effect of pH, the concentration of U-DFO was 36 μM. For the experiments investigating the impact of U-DFOB concentration at a constant pH, the concentrations of U-DFOB were in the range of 6–78 μM. No further pH drift was observed after these additions, and all suspensions were allowed to mix for an additional 24 h. The samples were then centrifuged for 10 min at 5000 rpm (Thermo Scientific, Sorvall™ ST 16), and small aliquots were isolated from the supernatant to determine the total uranium, DFO, and Mn^{2+} in the aqueous phase. This procedure was repeated for control adsorption experiments, which contained only DFO and U(VI) solutions separately. All experiments were performed in triplicate.

2.4. Elemental and DFOB Analysis

The total manganese and uranium concentrations in the supernatant were analyzed using ICP-MS (Thermo Scientific, iCAP R.Q.). Calibration standards were prepared from manganese and uranium standard solutions (Alfa Aesar, SpecPure™ plasma standard solution in 5% HNO_3) with concentrations of 0.1–19 μg L^{-1} and 10–500 μg L^{-1}, respectively. All solutions (calibration standards and samples) were diluted using plasma grade 2% HNO_3 (Thermo Scientific).

The concentration of DFO present in the supernatant was determined spectrophotometrically via UV-vis spectroscopy using $FeCl_3$ (Alfa Aesar, 99% purity) [40,50]. Specifically, amounts of $FeCl_3$ in 0.1 M HCl in excess were added to aliquots of the supernatant in 4.5 mL polystyrene cuvettes and diluted with deionized water to a final volume of 2.6 mL. These samples were capped and allowed to sit for 10 min, and the Fe-DFO complex's absorbance was measured at 428 nm. This procedure determined $[DFO]_{Total}$ in the supernatant as Fe(III) forms complexes with any non-complexed DFO in the solution as well as any DFO complexed with U(VI) since Fe(III) forms a stronger complex with DFOB ($\log \beta = 32.02 \pm 0.5$) compared to U(VI) ($17.1 \pm 0.2$) [41]. The metal exchange was kinetically swift and quantitative: the U-DFO stock solution of a known concentration was reacted with $FeCl_3$ and yielded 100% DFO recovery. Calibration standards of Fe(III)-DFO were made by adding stock 1 mM DFO with at least a 1:1 molar equivalent of $FeCl_3$ and was diluted to achieve a calibration range of 1.9 μM to 13.5 μM of Fe(III)-DFO. No spectra interferences were observed by U(VI) and U-DFO under the conditions studied.

2.5. Determination of Acetate and Succinate

Standards of acetate and succinate were prepared using sodium acetate anhydrous (Thermo Scientific, ≥99% purity) and sodium succinate dibasic (Sigma Aldrich (St. Louis, MO, USA), 98% purity) stock solutions, with concentrations ranging from 0.3 to 5 ppm. Retention times in ion chromatography for acetate and succinate were at 6.1 and 4.6 min, respectively. Due to pH adjustments and mesylate salt exchange, chloride ions were present, and no interferences were observed at 3.8 min in the determination of acetate and succinate.

3. Results and Discussion

3.1. DFOB vs. DFOD

The interaction of compounds with the pyrolusite surface for this preliminary study was determined through concentrations before and after sorption. The subsequent disappearance of intact molecules in the supernatant was considered to be adsorbed on the mineral surface. This paper identified complexation via DFO concentrations (UV-Vis) and

uranium concentrations (ICP-MS) to provide a complete depiction of the system from multiple assessments. Figure 2 illustrates the percentage of sorption from DFO controls and complexes through DFO concentrations on the left in Figure 2a. Conversely, Figure 2b on the right shows the percentage of sorption experienced by the uranium control and complexes through uranium concentrations. The uranium control for DFOB and DFOD was the same; accordingly, it is only shown here once. Control samples at pH 6 revealed DFOB sorption on the surface at 52% (Figure 2a light blue horizontal) vs. DFOD at 29% (Figure 2a dark blue diagonal). This difference indicates the importance of the amino group on DFOB when considering surface interactions since this is the only structural difference between the two molecules. Concurrently, the amount of uranium from the same samples revealed a minor increase of 7% to DFO, which, under these conditions, is not conclusive evidence that complexation definitively enhances sorption (Figure 2b).

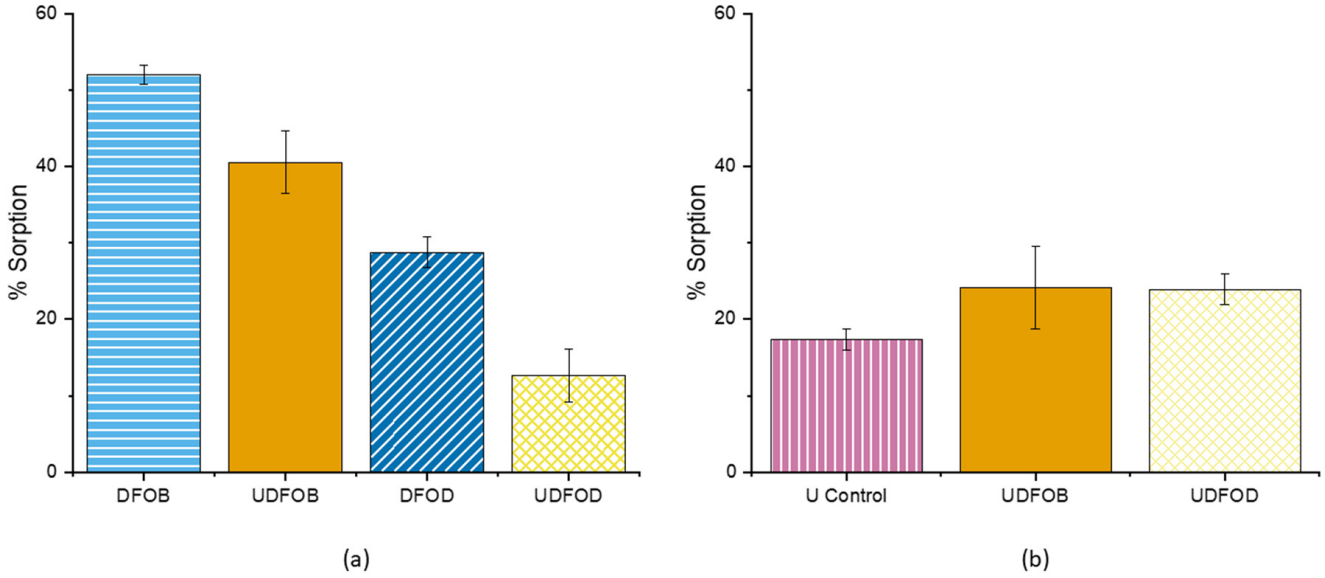

Figure 2. Sorption percentage at pH 6 for: (**a**) DFOB to pyrolusite with solutions containing DFOB only (light blue horizontal), DFOD only (dark blue diagonal), and complexed solutions of U-DFOB (orange solid) and U-DFOD (yellow crosshatch); (**b**) Uranium sorption to pyrolusite with solutions containing only U(VI) (pink vertical) and complexed solutions of U-DFOB (orange solid) and U-DFOD (yellow crosshatch). Error bars represent standard deviation.

When comparing the complexation results from both DFO sorption and U(VI) sorption, it can also be noted that these two components did not disappear with the same amount of samples. The 41% sorption of the DFOB complex (Figure 2a orange solid) was higher than the 24% sorption shown by U-DFOB (Figure 2b orange solid), indicating that uncomplexed DFOB sorbs to the surface along with U-DFOB. The opposite is true of DFOD, with uncomplexed U(VI) sorbing to the surface along with U-DFOD due to the 24% uranium concentration (Figure 2b yellow crosshatch) being higher than the 13% DFOD concentration (Figure 2a yellow crosshatch). The interaction between DFOB and U(VI) is not exclusively due to the sorption of an intact U-DFOB complex; the sorption pathways are discussed below.

3.2. DFOB pH 6 vs. pH 8

The overall trend of less complex sorption relative to the control remains the same when comparing the differences in DFOB from pH 6 to pH 8 (Figure 3a). The U-DFOB (Figure 3a orange solid) sorbs to the surface less than DFOB (Figure 3a blue horizontal) by itself. It is reasonable that the uranyl ion in the solution in the absence of DFOB has a higher sorption at pH 8 than pH 6 (Figure 3b pink vertical). Showing higher metal sorption at higher pH could be attributed to the increase in a negative charge on the mineral surface and has been observed with pyrolusite and other metals, Tl(I), Pb(II), Zn(II),

Mg(II), Cd(II) [51,52]. When comparing pH 8's complex results, DFOB sorption (Figure 3a orange solid) and U(VI) sorption (Figure 3b orange solid) established that no species sorbed more to the surface than the complex.

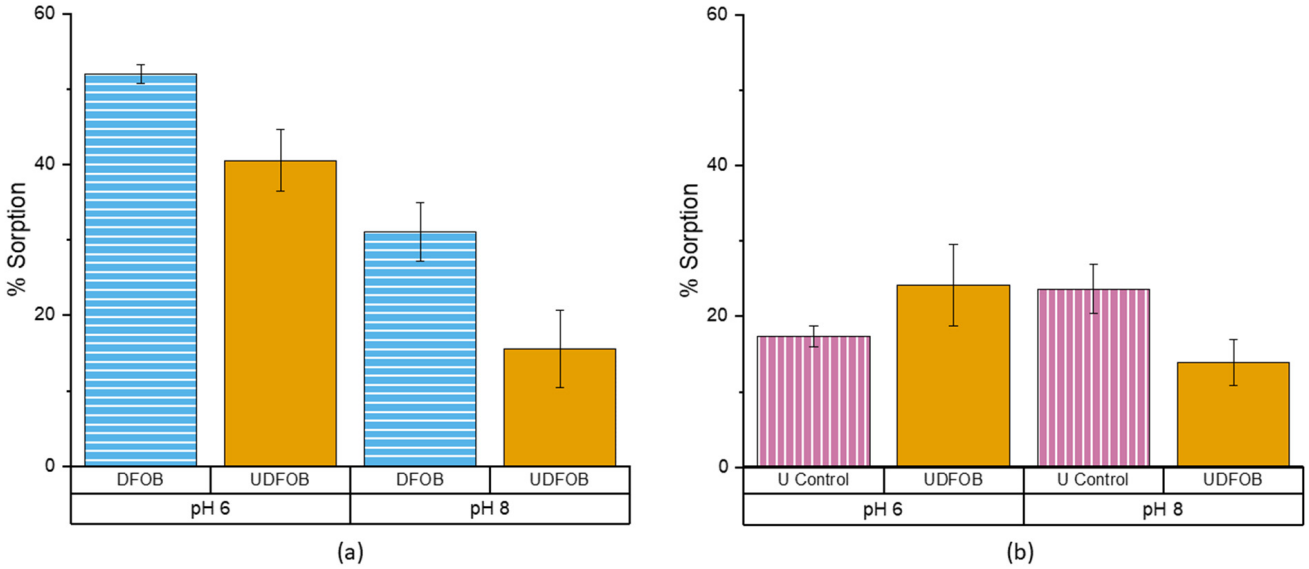

Figure 3. Sorption percentage at pH 6 and 8 to pyrolusite with (**a**) Solutions containing only DFOB (light blue horizontal) complexed with U(VI) (orange solid); (**b**) Solutions containing only U(VI) (pink vertical) complexed with DFOB (orange solid). Error bars represent standard deviation.

Across the pH range studied, the speciation of both un-complexed DFOB and U-DFOB was unlikely to contribute to the difference in sorption. The un-complexed DFOB exists as one species with three hydroxamic groups (protonated hydroxamates) and a protonated terminal amine group, providing an overall positive charge of one throughout the pH range of this study. Mullen et al. examined the speciation of the U-DFOB complex through a pH range of 3–10 and determined the existence of three major U-DFOB species [12]. At pH 6 and 8, the dominant species was UO_2DFOBH, with a minor species at pH 8 of the uranyl mono hydroxide species UO_2OHDFOBH. The dominant species at both pH 6 and 8 was neutral; however, they still contained a protonated terminal amine group as a localized positive charge source. While electrostatic interactions were expected, there must also be additional mechanisms for sorption that do not rely on the pH-dependent characteristics of the substrate.

3.3. Ligand-Metal Adsorption Mechanisms

In the literature, three frequently mentioned orientations for the adsorption of metal–ligand complexes onto mineral surfaces are summarized in Figure 4 [53–57].

Type 1 functions when the metal directly absorbs the mineral if the mineral has exchangeable or appropriately charged surface groups and the coordination shell of the metal is not filled. This mechanism did not describe our experimental results since Figures 2 and 3 show that U(VI) did not drive DFO sorption and all 3 hydroxamate groups complex with U(VI) [54].

Type 2 orientation involves a ligand adsorbing directly to the mineral surface and has additional active groups that are capable of forming a ligand bridge between the surface and the metal cation. Adsorption in this manner is "ligand-like", with increasing adsorption as the pH decreases [53]. In Type 3, the metal and ligand can sorb while remaining complexed on the mineral surface if surface sites are in close enough proximity. This leads to adsorption that exhibits both "metal-like" and "ligand-like" behaviors [53]. It can be stated that Type 3 is the proper mechanism over Type 2 with properties of 2 and then more than exclude 2. First, the assertion for the properties of Type 2 is discussed.

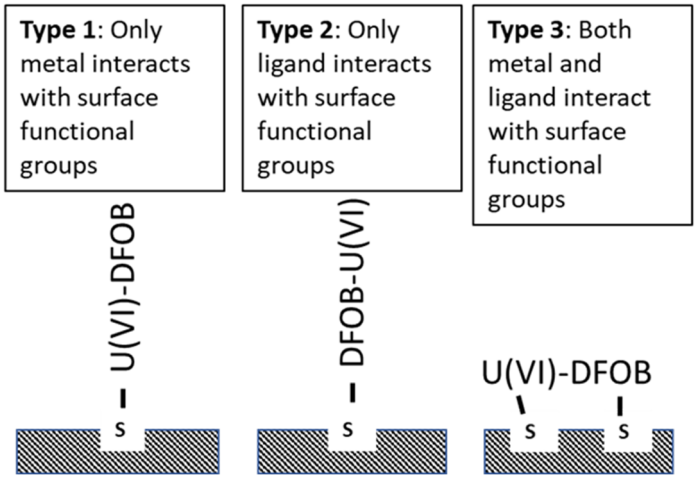

Figure 4. Plausible adsorption mechanisms of metal-ligand complexes. Type 1 involves adsorption through the metal, Type 2 is only through ligand active groups, and Type 3 consists of the interaction of both metal and ligand active groups to the surface [53].

3.4. Type 2 Ligand-like Mechanism

The mechanism of sorption of DFOB has been well studied previously on various substrates under different environmental conditions [29,40,45,49,58,59]. Siebner-Freibach et al. (2006) examined the adsorption of free DFOB and Fe(III)-DFOB onto a Ca-montmorillonite through thermospectroscopic studies. The free ligand was adsorbed using all active groups, with hydroxamic carbonyl and hydroxyl oxygens, hydrogen bonding with the N-H of the secondary amide groups, and, as stated previously, through NH_3^+ adsorption directly onto the surface or indirectly through water molecules (Figure 5) [29]. When binding occurred through the terminal amine or secondary amide groups, it was shown through FTIR that the Fe-binding center (hydroxamate groups) was unaffected [29]. DFO coordinates with Fe(III) to form a hexadentate octahedral complex using its three hydroxamate groups, and it is expected to coordinate with UO_2^{2+} in a similar manner [28,41,60]. In this instance, DFOB sorbs onto the surface of pyrolusite through the NH_3^+ and/or secondary amide groups, allowing UO_2^{2+} to become sequestered on the surface while staying complexed to DFOB. This is highlighted with sorption comparisons between complexed DFO. The 28% decrease in sorption proceeding from U-DFOB to U-DFOD (Figure 2a light blue horizontal—dark blue diagonal) indicates the key role of terminal amine displaying ligand-like behavior. As DFOD still displays sorption, when un-complexed and complex, the contribution of secondary amines in sorption is not to be discounted. The adsorption of U(VI), when complex, to the surface through NH_3^+ or the secondary amine group can be equated to $[U(VI)]_{sorbed}$.

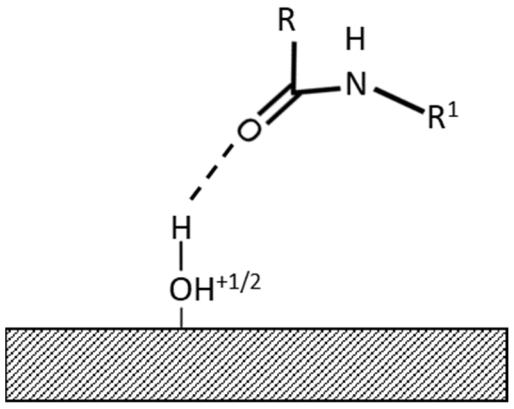

Figure 5. Secondary amine group in DFO hydrogen bonding with hydroxylated surface groups.

3.5. Type 3 Ligand-like and Metal-like Mechanism

Both acetate and succinate were detected in the supernatant under the conditions studied with the amount of acetate and succinate released, as shown in Figure 6. Acetate indicates hydrolysis and subsequent DFOB oxidation. The additional presence of succinate in the samples suggests that the oxidation/hydrolysis reaction results in the multi-step degradation of DFOB via inner-sphere binding to pyrolusite, where the molecule is no longer left intact to complex with metals [61]. In addition, acetate and succinate are not likely to adsorb onto the pyrolusite surface. It can be concluded that the acetate and succinate detected in the solution represent all the hydrolysis products of DFOB and, therefore, reflect every DFOB molecule that participates in inner-sphere complexation and the resultant hydrolysis/reducing reaction [62]. The DFOB that undergoes hydrolysis is not considered to be adsorbed on the surface and is referred to as $DFOB_{Hydrolyzed}$.

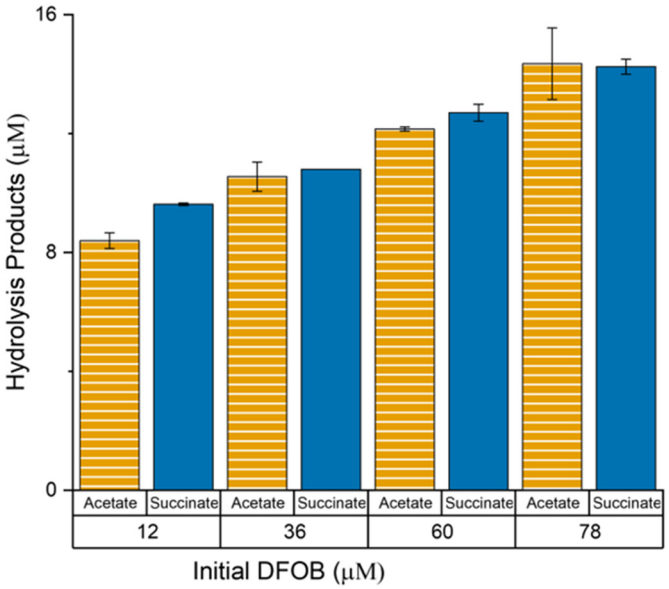

Figure 6. Acetate (orange horizontal) and succinate (dark blue solid) released into the solution at pH 6. Error bars represent the relative standard deviation from triplicate samples.

The sorption of DFOB has been attributed to the dissolution and subsequent release of structural Fe(III) and Mn(II)/Mn(III) from iron (hydr)oxides and manganese oxides, which indicates that DFOB also takes part in reductive-promoted and ligand-promoted dissolution [40,49,58,63,64]. The presence of Mn(II) in the supernatant, post-sorption with DFOB, acts as the reducing agent of Mn(IV). All manganese present in the supernatant is assumed to be Mn(II) due to the reductive dissolution being the primary pathway for pH $\leq$ 6.5 [40]. The Mn(III)-DFOB complex is also unstable below pH 7.5, meaning that manganese detected in the supernatant must be in the +2 oxidation state [65]. Upon sorption with DFOB, Mn(IV) centered in pyrolusite acts similarly to the decomposing Mn(III)-DFOB complex and undergoes an internal electron transfer to provide Mn(II) and oxidized DFOB products.

Figure 7 shows this release of Mn(II) into the supernatant. The concentration of DFOB responsible for inner-sphere complexation with the mineral could be equated to the concentration of acetate detected in the aqueous phase. When pyrolusite was brought into contact with U(VI) (absence of DFOB), there was no release of Mn(II) into the solution. This corresponds to meager amounts of U(VI) sorption in the absence of DFOB. The U(VI) is not a reducing agent for Mn(IV) and does not promote the dissolution of the mineral. Pyrolusite in contact with DFOB, un-complexed and complex, leads to the significant release of Mn(II) into the solution. There is a direct correlation between the concentration of $DFOB_{hydrolyzed}$ ([acetate]) and the amount of Mn(II) released, and it has been determined that DFOB is the primary source of Mn(II) release into the solution. While this linear correlation of

inner-spherically complexed DFOB and the subsequent release of Mn(II) has been observed, the exact ratio of DFOB to Mn(II) is unknown. It is unclear how many hydroxamate groups bind inner-spherically or how many metal centers participate in coordination. In this study, approximately four Mn(II) atoms were released into the solution for every DFOB molecule that was inner-spherically adsorbed to the surface.

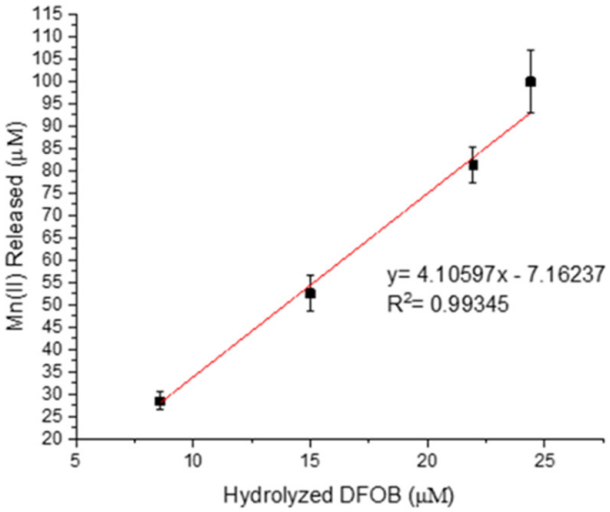

Figure 7. Concentration of Mn(II) released from the inner-sphere adsorption of DFOB at pH 6 as a function of hydrolyzed DFOB. The hydrolyzed DFOB concentration was set equal to the concentration of acetate in the samples. A linear fit was applied to obtain the slope. Error bars represent the relative standard deviation from triplicate samples.

The U-DFOB complex has three hydroxamate groups bound to the U(VI) and is initially unavailable for inner-sphere adsorption. Upon contact with the mineral surface, hydroxamate groups must be made available for the reduction in Mn(IV), which hydrolyzes DFOB to release Mn(II) and acetate. This points to the metal-like behavior of the system to match with the Type III mechanism. Furthermore, it explains why DFOB is missing from the supernatant (41%) at a greater amount than U(VI) (24%), as the siderophore must release the metal to proceed through this process. It has been hypothesized that a significant portion of the now uncomplexed DFOB remains attached to the surface with its terminal amine and/or secondary amides, while U(VI) is released into the supernatant with a minority remaining on the surface.

Combining the Type 2 mechanism with the inner-sphere mechanism allows for DFOB to be accounted for in the system. DFOB was initially introduced into the system and did not react with the surface of pyrolusite recovered in the supernatant, which was denoted as $[DFOB]_{supernatant}$. Some DFOB adsorbed inner-spherically onto the substrate, resulting in the hydrolysis producing acetate and succinate. Since the hydrolysis reaction included acetate in a 1:1 ratio with DFOB, the concentration of DFOB adsorbing inner spherically was equal to [acetate] [61]. The final portion of DFOB remained adsorbed onto the mineral surface, either electrostatically through the terminal amine group or hydrogen bonded through the secondary amide group. This mechanism is presumed to be the same mechanism by which U-DFOB also adsorbs to the surface; therefore, this portion of DFOB was set equal to the amount of U(VI) missing from the supernatant $[U(VI)]_{sorbed}$. These three portions of DFOB should account for the total amount of DFOB initially introduced into the system, $[DFOB]_{total}$. Table 1 shows how adding these portions together provides comparable values to the $[DFOB]_{total}$. In this analysis, a 1:1 ratio was assumed for U(VI) to DFOB; however, not every DFOB molecule adsorbed in this manner can be complex to U(VI). The proposed mechanisms in the mass balance account for both Type II and III anticipated DFOB adsorption mechanisms.

Table 1. Mass balance of DFOB after sorption onto pyrolusite at pH 6.

$[DFOB]_{supernatant}$ (μM)	[Acetate] (μM)	$[U(VI)]_{sorbed}$ (μM)	$[DFOB]_{supernatant}$ + [Acetate] + $[U(VI)]_{sorbed}$ (μM)	$[DFOB]_{total}$ (μM)
37.44	14.35	24.4	76.19 (±4.00)	78
26.206	12.15	21.95	60.31 (±4.45)	60
14.01	10.55	15.0	39.56 (±0.75)	37
2.02	8.40	8.59	19.01 (±0.36)	12

4. Conclusions

Both inner-sphere coordination and electrostatic interactions with the hydroxamate and secondary amine groups confirm the possibility of a Type II and III mechanism. Removing the positive terminal charge by involving DFOD in the experiment allowed the Type II mechanism to be defined. The 23% difference in sorption between DFOB and DFOD conveyed how the terminal amine plays a significant role in the sorption of DFOB. However, the DFOD and U-DFOD complex could still sorb to the surface without a positive charge on their end. This eliminates the possibility of the terminal amine being the sole source of sorption and reinforces the inner-sphere coordination premise where middle groups play a crucial role in the mechanism. This experiment presents Type III as the concluding mechanism for the ternary system of DFOB with U(VI) onto a manganese mineral surface by exhibiting behaviors beyond that expected from Type II alone.

As a notable contaminant with the potential for severe damage to biological systems and a long half-life, the environmental fate of uranium must be controlled. It is essential for remediation strategies based on environmental models to include manganese minerals and DFOB as they both disturb systems disproportionately to their concentrations. It is essential for future studies to consider the propensity for inherent molecules, such as siderophores from bacteria and fungi, to modify the mobilization of radionuclides The interplay of sorption involves a mix of complicated systems that must be further understood to make safe and dutiful decisions.

Author Contributions: Methodology, M.S., L.H., B.J. and V.A.; Software, M.S., L.H. and J.S.; Validation, M.S., L.H., J.S. and I.S.; Formal analysis, M.S. and L.H.; Investigation, M.S. and L.H.; Resources, V.A.; Data curation, M.S. and L.H.; Writing—original draft, M.S.; Writing—review & editing, L.H.; Visualization, M.S. and L.H.; Supervision, V.A.; Project administration, V.A.; Funding acquisition, V.A. All authors have read and agreed to the published version of the manuscript.

Funding: This research was funded by the Nuclear Regulatory Commission (NRC) under award 31310019M0010.

Data Availability Statement: The data presented in this study are available on request from the corresponding author.

Conflicts of Interest: The authors declare no conflict of interest.

References

1. Sprynskyy, M.; Kowalkowski, T.; Tutu, H.; Cukrowska, E.M.; Buszewski, B. Adsorption Performance of Talc for Uranium Removal from Aqueous Solution. *Chem. Eng. J.* **2011**, *171*, 1185–1193. [CrossRef]
2. Maher, K.; Bargar, J.R.; Brown, G.E. Environmental Speciation of Actinides. *Inorg. Chem.* **2013**, *52*, 3510–3532. [CrossRef]
3. Walther, C.; Denecke, M.A. Actinide Colloids and Particles of Environmental Concern. *Chem. Rev.* **2013**, *113*, 995–1015. [CrossRef]
4. Anagnostopoulos, V.; Katsenovich, Y.; Lee, B.; Lee, H.M. Biotic Dissolution of Autunite under Anaerobic Conditions: Effect of Bicarbonates and Shewanella Oneidensis MR1 Microbial Activity. *Environ. Geochem. Health* **2020**, *42*, 2547–2556. [CrossRef] [PubMed]
5. Salbu, B.; Kashparov, V.; Lind, O.C.; Garcia-Tenorio, R.; Johansen, M.P.; Child, D.P.; Roos, P.; Sancho, C. Challenges Associated with the Behaviour of Radioactive Particles in the Environment. *J. Environ. Radioact.* **2018**, *186*, 101–115. [CrossRef]
6. Agency for Toxic Substances and Disease Registry ATSDR. *Toxicological Profile for Plutonium*; Department of Health and Human Services: Atlanta, GA, USA, 2010.
7. Agency for Toxic Substances and Disease Registry ATSDR. *Toxicological Profile for Uranium*; Department of Health and Human Services: Atlanta, GA, USA, 2013.

8. Szlamkowicz, I.; Stanberry, J.; Lugo, K.; Murphy, Z.; Ruiz Garcia, M.; Hunley, L.; Qafoku, N.P.; Anagnostopoulos, V. Role of Manganese Oxides in Controlling Subsurface Metals and Radionuclides Mobility: A Review. *ACS Earth Space Chem.* **2023**, *7*, 1–10. [CrossRef]
9. Gavrilescu, M.; Pavel, L.V.; Cretescu, I. Characterization and Remediation of Soils Contaminated with Uranium. *J. Hazard. Mater.* **2009**, *163*, 475–510. [CrossRef] [PubMed]
10. Environmental Management Support, Inc. *Innovative Remediation Remediation Technologies: Field-Scale Demonstration Projects in North America*, 2nd ed.; Environmental Protection Agency: Washington, DC, USA, 2000.
11. Szlamkowicz, I.B.; Fentress, A.J.; Longen, L.F.; Stanberry, J.S.; Anagnostopoulos, V.A. Transformations and Speciation of Iodine in the Environment as a Result of Oxidation by Manganese Minerals. *ACS Earth Space Chem.* **2022**, *6*, 1948–1956. [CrossRef]
12. Stanberry, J.; Szlamkowicz, I.; Purdy, L.R.; Anagnostopoulos, V. TcO2 Oxidative Dissolution by Birnessite under Anaerobic Conditions: A Solid–Solid Redox Reaction Impacting the Environmental Mobility of Tc-99. *Environ. Sci. Process. Impacts* **2021**, *23*, 844–854. [CrossRef]
13. Stanberry, J.; Szlamkowicz, I.; Magno, D.; Shultz, L.; Anagnostopoulos, V. Oxidative Dissolution of TcO2 by Mn(III) Minerals under Anaerobic Conditions: Implications on Technetium-99 Remediation. *Appl. Geochem.* **2021**, *127*, 104858. [CrossRef]
14. Wu, W.-M.; Carley, J.; Fienen, M.; Mehlhorn, T.; Lowe, K.; Nyman, J.; Luo, J.; Gentile, M.E.; Rajan, R.; Wagner, D.; et al. Pilot-Scale in Situ Bioremediation of Uranium in a Highly Contaminated Aquifer. 1. Conditioning of a Treatment Zone. *Environ. Sci. Technol.* **2006**, *40*, 3978–3985. [CrossRef] [PubMed]
15. Kraemer, S.M. Iron Oxide Dissolution and Solubility in the Presence of Siderophores. *Aquat. Sci. Res. Across Boundaries* **2004**, *66*, 3–18. [CrossRef]
16. Liermann, L.J.; Kalinowski, B.E.; Brantley, S.L.; Ferry, J.G. Role of Bacterial Siderophores in Dissolution of Hornblende. *Geochim. Cosmochim. Acta* **2000**, *64*, 587–602. [CrossRef]
17. Saha, M.; Sarkar, S.; Sarkar, B.; Sharma, B.K.; Bhattacharjee, S.; Tribedi, P. Microbial Siderophores and Their Potential Applications: A Review. *Environ. Sci. Pollut. Res.* **2016**, *23*, 3984–3999. [CrossRef]
18. Saha, R.; Saha, N.; Donofrio, R.S.; Bestervelt, L.L. Microbial Siderophores: A Mini Review: Microbial Siderophores. *J. Basic Microbiol.* **2013**, *53*, 303–317. [CrossRef]
19. Haas, H. Molecular Genetics of Fungal Siderophore Biosynthesis and Uptake: The Role of Siderophores in Iron Uptake and Storage. *Appl. Microbiol. Biotechnol.* **2003**, *62*, 316–330. [CrossRef]
20. Braud, A.; Geoffroy, V.; Hoegy, F.; Mislin, G.L.A.; Schalk, I.J. Presence of the Siderophores Pyoverdine and Pyochelin in the Extracellular Medium Reduces Toxic Metal Accumulation in Pseudomonas Aeruginosa and Increases Bacterial Metal Tolerance: Extracellular Sequestration of Toxic Metals by Siderophores. *Environ. Microbiol. Rep.* **2010**, *2*, 419–425. [CrossRef]
21. Farkas, E.; Csóka, H.; Micera, G.; Dessi, A. Copper(II), Nickel(II), Zinc(II), and Molybdenum(VI) Complexes of Desferrioxamine B in Aqueous Solution. *J. Inorg. Biochem.* **1997**, *65*, 281–286. [CrossRef]
22. Aoki, J.; Oonuma, C.; Sudowe, R.; Takagai, Y. Adsorption Behavior of Pu(IV), Am(III), Cm(III), and U(VI) on Desferrioxamine B-Immobilized Micropolymer and Its Applications in the Separation of Pu(IV). *Anal. Sci.* **2021**, *37*, 1641–1644. [CrossRef]
23. Kenney, J.P.L.; Ellis, T.; Nicol, F.S.; Porter, A.E.; Weiss, D.J. The Effect of Bacterial Growth Phase and Culture Concentration on U(VI) Removal from Aqueous Solution. *Chem. Geol.* **2018**, *482*, 61–71. [CrossRef]
24. Bellotti, D.; Remelli, M. Deferoxamine B: A Natural, Excellent and Versatile Metal Chelator. *Molecules* **2021**, *26*, 3255. [CrossRef] [PubMed]
25. Hofmann, M.; Retamal-Morales, G.; Tischler, D. Metal Binding Ability of Microbial Natural Metal Chelators and Potential Applications. *Nat. Prod. Rep.* **2020**, *37*, 1262–1283. [CrossRef] [PubMed]
26. Ahmed, E.; Holmström, S.J.M. Siderophores in Environmental Research: Roles and Applications: Siderophores in Environmental Research. *Microb. Biotechnol.* **2014**, *7*, 196–208. [CrossRef] [PubMed]
27. Snow, G.A. Metal Complexes of Mycobactin P and of Desferrisideramines. *Biochem. J.* **1969**, *115*, 199–205. [CrossRef]
28. Dhungana, S.; White, P.S.; Crumbliss, A.L. Crystal Structure of Ferrioxamine B: A Comparative Analysis and Implications for Molecular Recognition. *J. Biol. Inorg. Chem.* **2001**, *6*, 810–818. [CrossRef]
29. Siebner-Freibach, H.; Hadar, Y.; Yariv, S.; Lapides, I.; Chen, Y. Thermospectroscopic Study of the Adsorption Mechanism of the Hydroxamic Siderophore Ferrioxamine B by Calcium Montmorillonite. *J. Agric. Food Chem.* **2006**, *54*, 1399–1408. [CrossRef]
30. Tebo, B.M.; Bargar, J.R.; Clement, B.G.; Dick, G.J.; Murray, K.J.; Parker, D.; Verity, R.; Webb, S.M. BIOGENIC MANGANESE OXIDES: Properties and Mechanisms of Formation. *Annu. Rev. Earth Planet. Sci.* **2004**, *32*, 287–328. [CrossRef]
31. Post, J.E.; McKeown, D.A.; Heaney, P.J. Raman Spectroscopy Study of Manganese Oxides: Tunnel Structures. *Am. Mineral.* **2020**, *105*, 1175–1190. [CrossRef]
32. Birkner, N.; Navrotsky, A. Thermodynamics of Manganese Oxides: Sodium, Potassium, and Calcium Birnessite and Cryptomelane. *Proc. Natl. Acad. Sci. USA* **2017**, *114*, E1046–E1053. [CrossRef]
33. Ma, W.; Kwan, K.W.; Wu, R.; Ngan, A.H.W. High-Performing, Linearly Controllable Electrochemical Actuation of c-Disordered δ-MnO_2/Ni Actuators. *J. Mater. Chem. A* **2021**, *9*, 6261–6273. [CrossRef]
34. Bi, X.; Tang, T.; Meng, X.; Gou, M.; Liu, X.; Zhao, P. Aerobic Oxidative Dehydrogenation of N-Heterocycles over OMS-2-Based Nanocomposite Catalysts: Preparation, Characterization and Kinetic Study. *Catal. Sci. Technol.* **2020**, *10*, 360–371. [CrossRef]

35. Yao, N.; Zhao, H.; Liu, X.; Serol Ertürk, A.; Elmaci, G.; Zhao, P.; Meng, X. Synergistic Adsorption and Oxidative Degradation of Polyvinyl Alcohol by Acidified OMS-2: Catalytic Mechanism, Degradation Pathway and Toxicity Evaluation. *Sep. Purif. Technol.* **2022**, *302*, 122047. [CrossRef]
36. Wang, X.; Bi, X.; Yao, N.; Elmaci, G.; Serol Ertürk, A.; Lv, Q.; Zhao, P.; Meng, X. Doping Strategy-Tuned Non-Radical Pathway on Manganese Oxide for Catalytic Degradation of Parabens. *Chem. Eng. J.* **2022**, *442*, 136180. [CrossRef]
37. Minakshi, M.; Mitchell, D.; Prince, K. Incorporation of TiB_2 Additive into MnO_2 Cathode and Its Influence on Rechargeability in an Aqueous Battery System. *Solid State Ion.* **2008**, *179*, 355–361. [CrossRef]
38. Jenne, E.A. *Trace Inorganics in Water*; Advances in Chemistry; Baker, R.A., Ed.; American Chemical Society: Washington, DC, USA, 1968; Volume 73, ISBN 978-0-8412-0074-6.
39. Post, J.E. Manganese Oxide Minerals: Crystal Structures and Economic and Environmental Significance. *Proc. Natl. Acad. Sci. USA* **1999**, *96*, 3447–3454. [CrossRef] [PubMed]
40. Duckworth, O.W.; Sposito, G. Siderophore−Manganese(III) Interactions II. Manganite Dissolution Promoted by Desferrioxamine B. *Environ. Sci. Technol.* **2005**, *39*, 6045–6051. [CrossRef]
41. Mullen, L.; Gong, C.; Czerwinski, K. Complexation of Uranium (VI) with the Siderophore Desferrioxamine B. *J. Radioanal. Nucl. Chem.* **2007**, *273*, 683–688. [CrossRef]
42. Kraemer, D.; Kopf, S.; Bau, M. Oxidative Mobilization of Cerium and Uranium and Enhanced Release of "Immobile" High Field Strength Elements from Igneous Rocks in the Presence of the Biogenic Siderophore Desferrioxamine B. *Geochim. Cosmochim. Acta* **2015**, *165*, 263–279. [CrossRef]
43. Takahashi, A.; Igarashi, S. Solvent Extraction of Uranium (IV) with Desferrioxamine B and Its Application to the Homogenous Liquid-Liquid Extraction Method Using a Fluorosurfactant. *Solvent Extr. Res. Dev.* **1999**, *6*, 61–71.
44. Hafez, M.B.; Hafez, N. Spectrophotometric Determination of Ce(IV), Fe(III) and U(VI) Using Desferrioxamine B (Desferal). *J. Chem. Technol. Biotechnol.* **2007**, *54*, 267–269. [CrossRef]
45. Neubauer, U.; Nowack, B.; Furrer, G.; Schulin, R. Heavy Metal Sorption on Clay Minerals Affected by the Siderophore Desferrioxamine B. *Environ. Sci. Technol.* **2000**, *34*, 2749–2755. [CrossRef]
46. Kirby, M.E.; Watson, J.S.; Najorka, J.; Kenney, J.P.L.; Krevor, S.; Weiss, D.J. Experimental Study of PH Effect on Uranium (UVI) Particle Formation and Transport through Quartz Sand in Alkaline 0.1 M Sodium Chloride Solutions. *Colloids Surf. A Physicochem. Eng. Asp.* **2020**, *592*, 124375. [CrossRef]
47. Kirby, M.; Weiss, D.J. A Pilot Study on the Effect of Desferrioxamine B on Uranium VI Precipitation and Dissolution in pH 11.5, 0.1 M NaCl Solutions. *J. Radioanal. Nucl. Chem.* **2022**, *331*, 1779–1784. [CrossRef]
48. Kraemer, S.M.; Cheah, S.-F.; Zapf, R.; Xu, J.; Raymond, K.N.; Sposito, G. Effect of Hydroxamate Siderophores on Fe Release and Pb(II) Adsorption by Goethite. *Geochim. Cosmochim. Acta* **1999**, *63*, 3003–3008. [CrossRef]
49. Simanova, A.A.; Persson, P.; Loring, J.S. Evidence for Ligand Hydrolysis and Fe(III) Reduction in the Dissolution of Goethite by Desferrioxamine-B. *Geochim. Cosmochim. Acta* **2010**, *74*, 6706–6720. [CrossRef]
50. Frazier, S.W.; Kretzschmar, R.; Kraemer, S.M. Bacterial Siderophores Promote Dissolution of UO2 under Reducing Conditions. *Environ. Sci. Technol.* **2005**, *39*, 5709–5715. [CrossRef] [PubMed]
51. Ajmal, M.; Rao, R.A.K.; Siddiqui, B.A. Adsorption Studies and the Removal of Dissolved Metals Using Pyrolusite as Adsorbent. *Environ. Monit. Assess.* **1995**, *38*, 25–35. [CrossRef]
52. Liu, J.; Lippold, H.; Wang, J.; Lippmann-Pipke, J.; Chen, Y. Sorption of Thallium(I) onto Geological Materials: Influence of PH and Humic Matter. *Chemosphere* **2011**, *82*, 866–871. [CrossRef] [PubMed]
53. Bowers, A.R.; Huang, C.P. Adsorption Characteristics of Metal-EDTA Complexes onto Hydrous Oxides. *J. Colloid Interface Sci.* **1986**, *110*, 575–590. [CrossRef]
54. Nowack, B.; Sigg, L. Adsorption of EDTA and Metal–EDTA Complexes onto Goethite. *J. Colloid Interface Sci.* **1996**, *177*, 106–121. [CrossRef] [PubMed]
55. Elliott, H.A.; Huang, C.P. The Adsorption Characteristics of Cu(II) in the Presence of Chelating Agents. *J. Colloid Interface Sci.* **1979**, *70*, 29–45. [CrossRef]
56. Benjamin, M.M.; Leckie, J.O. Conceptual Model for Metal-Ligand-Surface Interactions during Adsorption. *Environ. Sci. Technol.* **1981**, *15*, 1050–1057. [CrossRef]
57. Davis, J.A.; Leckie, J.O. Effect of Adsorbed Complexing Ligands on Trace Metal Uptake by Hydrous Oxides. *Environ. Sci. Technol.* **1978**, *12*, 1309–1315. [CrossRef]
58. Haack, E.A.; Johnston, C.T.; Maurice, P.A. Mechanisms of Siderophore Sorption to Smectite and Siderophore-Enhanced Release of Structural Fe^{3+}. *Geochim. Cosmochim. Acta* **2008**, *72*, 3381–3397. [CrossRef]
59. Rosenberg, D.R.; Maurice, P.A. Siderophore Adsorption to and Dissolution of Kaolinite at PH 3 to 7 and 22 °C. *Geochim. Cosmochim. Acta* **2003**, *67*, 223–229. [CrossRef]
60. Groenewold, G.S.; Van Stipdonk, M.J.; Gresham, G.L.; Chien, W.; Bulleigh, K.; Howard, A. Collision-Induced Dissociation Tandem Mass Spectrometry of Desferrioxamine Siderophore Complexes from Electrospray Ionization of UO^{22+}, Fe^{3+} and Ca^{2+} Solutions. *J. Mass Spectrom.* **2004**, *39*, 752–761. [CrossRef]
61. Winkelmann, G.; Busch, B.; Hartmann, A.; Kirchhof, G.; Süßmuth, R.; Jung, G. Degradation of Desferrioxamines by Azospirillum Irakense: Assignment of Metabolites by HPLC/Electrospray Mass Spectrometry. *BioMetals* **1999**, *12*, 255–264. [CrossRef]

62. Norén, K.; Persson, P. Adsorption of Monocarboxylates at the Water/Goethite Interface: The Importance of Hydrogen Bonding. *Geochim. Cosmochim. Acta* **2007**, *71*, 5717–5730. [CrossRef]
63. Duckworth, O.W.; Sposito, G. Siderophore-Promoted Dissolution of Synthetic and Biogenic Layer-Type Mn Oxides. *Chem. Geol.* **2007**, *242*, 497–508. [CrossRef]
64. Peña, J.; Duckworth, O.W.; Bargar, J.R.; Sposito, G. Dissolution of Hausmannite (Mn_3O_4) in the Presence of the Trihydroxamate Siderophore Desferrioxamine B. *Geochim. Cosmochim. Acta* **2007**, *71*, 5661–5671. [CrossRef]
65. Duckworth, O.W.; Sposito, G. Siderophore−Manganese(III) Interactions. I. Air-Oxidation of Manganese(II) Promoted by Desferrioxamine B. *Environ. Sci. Technol.* **2005**, *39*, 6037–6044. [CrossRef]